▊ **Porphyrin Chemistry** |*Hot Paper*|

A Synthetic Strategy for Cofacial Porphyrin-Based Homo- and Heterobimetallic Complexes

Christoph Schissler,[a] Erik K. Schneider,[b] Benjamin Felker,[a] Patrick Weis,[b] Martin Nieger,[c] Manfred M. Kappes,*[b, d] and Stefan Bräse*[a, e]

Abstract: We present a straightforward and generally applicable synthesis route for cofacially linked homo- and heterobimetallic porphyrin complexes. The protocol allows the synthesis of unsymmetrical aryl-based *meso-meso* as well as β-*meso*-linked porphyrins. Our method significantly increases the overall yield for the published compound known as *o*-phenylene-bisporphyrin (OBBP) by a factor of 6.8. Besides the synthesis of 16 novel homobimetallic complexes containing Mn^{III}, Fe^{III}, Ni^{II}, Cu^{II}, Zn^{II}, and Pd^{II}, we achieved the first single-crystal X-ray structure of an unsymmetrical cofacial benzene-linked porphyrin dimer containing both planar-chiral enantiomers of a Ni^{II}_2 complex. Additionally, this new methodology allows access to heterobimetallic complexes such as the Fe^{III}-Ni^{II} containing carbon monoxide dehydrogenase active site analogue. The isolated species were investigated by various techniques, including ion mobility spectrometry, DFT calculations, and UV/Vis spectroscopy. This allowed us to probe the influence of interplane distance on Soret band splitting.

Introduction

In nature, the catalytically active sites of metalloenzymes are often rigidly fixed structures in an adaptive protein matrix which defines a spatial arrangement of the metal-containing ligands relative to each other. In such systems, proximity of several metal cations is typically required to achieve catalytic func-

tion. Correspondingly, strongly interacting metal sites are the basis for the unique catalytic activity of many multinuclear metalloproteins such as hemocyanin,[1, 2] hemerythrin,[3] superoxide dismutase,[4] carbon monoxide dehydrogenase,[5] and cytochrome c oxidase.[6] To gain further understanding of the unique coordination chemistry of such complexes, one ideally needs a rigid molecular system that allows one to tune the distances between the different metal centers without also influencing them by significantly changing the ligand field. It then becomes possible to vary the interactions between metal centers, particularly those that give rise to cooperative catalytic effects, by slight variations of the rigid framework. One system of interest in this context is covalently linked dimeric porphyrin metal complexes that can be tuned by systematic structural variation and whose cooperative properties can be compared with those of the corresponding constituent monomers.

Porphyrins offer the opportunity to coordinate numerous different metal ions without changing ligands and can be synthesized in a tailor-made way.[7, 8] Stepwise syntheses are of especially great interest toward rationally accessing artificially made heterobimetallic active site analogues, for example, those of the above-mentioned enzymes. This makes dimeric porphyrins a perfect choice not only to model and understand elementary enzymatic reactivity, but also to study cooperative magnetic, catalytic, and optical properties of two spatially close-lying metal ions. In principle, three different bisporphyrin topologies are possible: coplanar, tilted, and cofacial. Cofacial orientation provides closer metal–metal separations and is therefore of greatest interest for cooperative effects.

Over the last fifty years, multiple synthetic routes have addressed cofacial bisporphyrins, starting with the synthesis of doubly urea and amide bridged *meso*-connected sandwich

[a] C. Schissler, B. Felker, S. Bräse
Institute of Organic Chemistry, Karlsruhe Institute of Technology (KIT)
Fritz-Haber-Weg 6, 76131 Karlsruhe (Germany)
E-mail: braese@kit.edu

[b] E. K. Schneider, P. Weis, M. M. Kappes
Institute of Physical Chemistry, Karlsruhe Institute of Technology (KIT)
Fritz-Haber-Weg 2, 76131 Karlsruhe (Germany)
E-mail: manfred.kappes@kit.edu

[c] M. Nieger
Department of Chemistry, University of Helsinki
P.O. Box 55, 00014 Helsinki (Finland)

[d] M. M. Kappes
Institute for Nanotechnology, Karlsruhe Institute of Technology (KIT)
Hermann-von-Helmholtz-Platz 1
76344 Eggenstein-Leopoldshafen (Germany)

[e] S. Bräse
Institute for Biological and Chemical Systems—Functional Molecular Systems, (IBCS-FMS), Karlsruhe Institute of Technology (KIT)
Hermann-von-Helmholtz-Platz 1
76344 Eggenstein-Leopoldshafen (Germany)

▭ Supporting information and the ORCID identification number(s) for the author(s) of this article can be found under:
https://doi.org/10.1002/chem.202002394.

Chemistry–A European Journal

Full Paper
doi.org/10.1002/chem.202002394

Chemistry Europe
European Chemical
Societies Publishing

porphyrin dimers by Collman and Chang.[9] Shortly thereafter, Collman et al. demonstrated electrocatalytic four-electron reduction of oxygen to water using cofacial binuclear cobalt porphyrins.[10] Inspired by this first bimetallic catalysis based on porphyrins, Reed and colleagues developed a novel synthetic route to imidazolate- and oxo-bridged metalloporphyrins in which only one linker moiety and one bridging ligand were needed.[11] Collman et al. then first synthesized dimeric β-linked face-to-face amide-bridged porphyrin dimers.[12]

At about the same time, Chang and Abdalmuhdi began to focus on cofacial porphyrin dimers connected via rigid linker moieties and prepared 8-anthryldiporphyrin by condensing two dipyrromethane derivatives at a linking anthracene moiety.[13] Later bisphenylenyldiporphyrin[14] and dibenzofuranyldiporphyrin[15] became available based on the same approach.

Parallel to the approaches using linker moieties that intrinsically favored cofacial orientations, Kobuke et al. developed a synthetic route to o-phenylene-bisporphyrins. Interestingly, these also showed a cofacial arrangement due to strong π-stacking interactions which can compensate for the 60° bite angle of the o-benzene linker.[16] Osuka et al. were able to conduct X-ray structure analyses of single crystals of 1,2-phenylene-bridged alkyl-porphyrin dimers, which proved the cofacial arrangement with an average plane separation of 3.43 Å.[17] Fletcher and Therien then established a new route toward cofacial porphyrin dimers via [2+2+2] cycloaddition of 1,6-heptadiyne with ethynyl-linked porphyrins.[18] They were able to synthesize meso-meso, meso-β, and β-β connected zinc complexes of cofacial porphyrin dimers by this method.[19] Through a novel Suzuki–Miyaura cross-coupling methodology toward cofacial bisporphyrins anchored by xanthene and dibenzofuran, starting with boronated porphyrin monomers, Nocera et al. facilitated the route developed earlier, to achieve porphyrin plane distances around 4 Å.[20] Since this publication in 2003, to our knowledge, there have been no further groundbreaking synthetic method developments on the way to spatially close cofacial porphyrins.

The pioneering syntheses described above suffer from quite modest overall yields. For example, the highest published yield for the overall synthesis of benzene-linked symmetrical porphyrin dimers is at the 0.65%[16] level. Furthermore, the procedures developed, for example, by Fletcher and Therien,[19] are not readily generalizable to the complexation of a wide range of different transition metal ions—in particular, heterobimetallic combinations. Therefore, in this study we aimed at developing a new high-yielding, tolerant, and robust synthetic methodology, which is suitable for both homo- and heterobimetallic cofacial bisporphyrin complexes and which allows for tunable metal–metal distances.

Results and Discussion

Homobimetallic complexes

We have developed a facile route to the three different cofacial ligands shown in Figure 1 (**1**, **2**, and **3**) starting with pyrrole
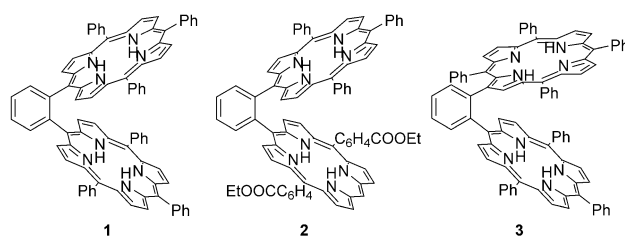
Figure 1. Targeted structures: **1**: o-phenylene-bisporphyrin (OBBP), **2**: o-phenylene-ethoxycarbonyl-bisporphyrin (EOBBP), **3**: o-phenylene-β-meso-bisporphyrin (BMOBBP). The molecules comprise porphyrin-based cofacial ligand systems which differ regarding the number and type of residues at meso-position and the connecting atom to the phenyl backbone.

and the corresponding aldehydes. The ligands differ regarding the number and type of residues in the meso-position as well as the position in which the porphyrin is connected to the phenyl backbone. The first two compounds require an asymmetric porphyrin as a starting point for the synthesis of the dimeric porphyrin-based ligands. Starting with a simple condensation reaction of pyrrole and paraformaldehyde dipyrromethane, **5** can be synthesized in up to 65% yield (Scheme 1). This can be used to build up the porphyrin cores **6** and **7** with the corresponding residues at the 5- and 15-positions depending on the aldehyde used. The next step is crucial for the distance between the porphyrin planes. Either the third meso-position is substituted by nucleophilic aromatic substitution with phenyllithium to obtain **8** or it remains unsubstituted. Monobromination with NBS under differing conditions then leads to bromo-porphyrin precursors **9** and **10**. On the way to ligand **3**, straightforward β-bromination of commercially available tetraphenylporphyrin (TPP) as the first step has to be conducted to afford **12**. The synthetic route via mono-brominated porphyrins as precursors enables incorporation of the benzene linker moiety without a second mixed-condensation as de-
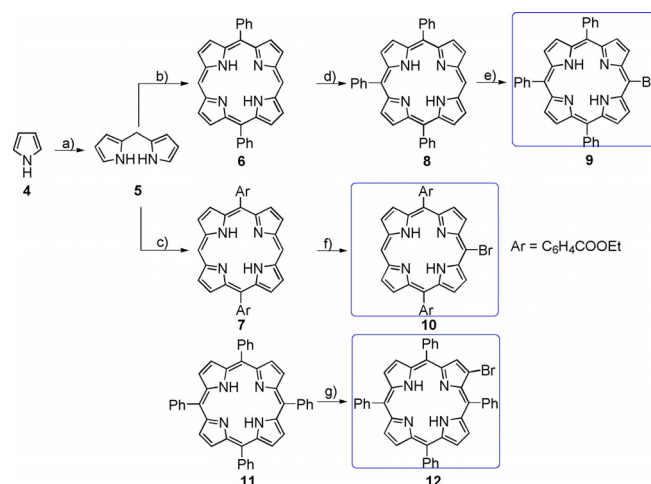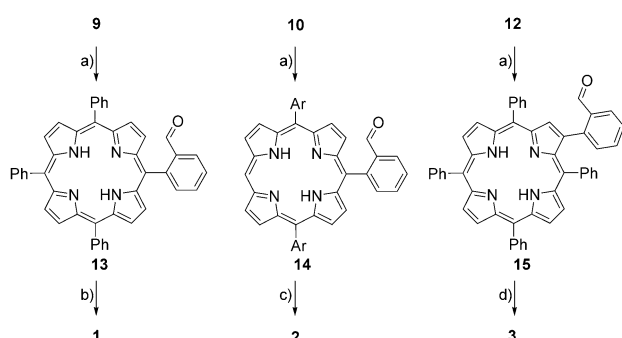
Scheme 1. Synthesis of brominated precursors: a) formaldehyde, InCl₃, NaOH, 55 °C, 3 h, 65%; b) benzaldehyde, TFA, DDQ, 4 h, 63%; c) ethyl-4-formylbenzoate, TFA, DDQ, 18 h, 53%, Ar: C₆H₄COOEt; d) PhLi, DDQ, THF, 0 °C→RT, 30 min, 95%; e) NBS, CH₂Cl₂, 0 °C→RT, 3 h, 97%; f) NBS, pyridine, CH₂Cl₂, 0 °C, 20 min, 60%; g) NBS, CH₂Cl₂, Δ, 8 h, 54%.

Chemistry–A European Journal

Full Paper
doi.org/10.1002/chem.202002394

Chemistry Europe
European Chemical
Societies Publishing

scribed,[16,17,21] but instead with the simple Suzuki–Miyaura cross-coupling reaction using 2-formylphenylboronic acid as the coupling counterpart as shown in Scheme 2.

In addition to that, asymmetric cofacial porphyrin dimers with one free *meso*-position have become available. Furthermore, bromination of one of the pyrrole carbon atoms enables the introduction of the backbone at the β-position which is not possible by conventional condensation reactions.

This robust procedure provides monomeric precursors in good overall yields (**13**: 26%, **14**: 12%, **15**: 28%). For compound **14** single crystals were obtained, which were suitable for X-ray crystallography (Figure 2). The molecular structure confirms the aldehyde functionality in the *o*-position of the anticipated linking moiety and clarifies that there should be enough space for the subsequent condensation reaction to obtain two cofacial porphyrin subunits linked together by an *o*-substituted phenyl bridge (Scheme 2).

The aldehyde functionalities of **13**, **14**, and **15** now take part in the concluding mixed condensation with pyrrole and benzaldehyde in a ratio of (1:4:3). As catalyst BF$_3$·OEt$_2$ or TFA were used, depending on the starting material. Crucial is the consecutive addition of pyrrole and benzaldehyde until the conversion of the aldehyde-porphyrins **13**, **14**, and **15**, as monitored by TLC, slows down. We achieve an increased yield by not sticking to the 1:4:3 ratio as the molecular structure suggested

because pyrrole and benzaldehyde prefer the condensation to TPP, excluding the aldehyde-porphyrins. Using an excess of pyrrole and benzaldehyde to achieve full conversion of the starting material is desirable, as TPP as a side product can easily be removed as the first purple fraction of the subsequent flash column chromatography on silica gel. Because the formation of the sterically less hindered TPP is observed before the bisporphyrin, even more sterically hindered porphyrin trimers could not be obtained by the described methodology.

The final condensations lead to the above shown cofacial porphyrin dimers. Our novel synthetic route to the known compound **1** increases its overall yield from 0.65%[16] or 0.30%[22] to 4.4% (i.e., by at least a factor of 6.8). The new compounds **2** and **3** could be synthesized in 1.9% and 1.3% yields, respectively. Whereas the final condensation of **1** and **2** rank within regular yields, for **3** the yield drops significantly. Besides steric issues faced during synthesis, the workup is aggravated due to higher basicity originating from the closer stacked porphyrin planes, which led to decreases in the isolated yield.

Note that in a similar 1,2-biphenylene-bridged porphyrin dimer, Osuka et al. showed by X-ray crystallography that the molecule has a near-parallel, cofacial porphyrin ring arrangement with a dihedral (twist) angle of 6.6° (see also schematic structure in the Supporting Information defining the dihedral angle).[17] In the absence of crystal structures, it is unclear whether **1**, **2**, and **3** have the same topology in the solid state. DFT calculations (on isolated molecules; see below) identify similarly cofacial benzene-linked porphyrin planes with dihedral angles between the porphyrins by way of the linker benzene hinge of 10.0° (OBBP), 0.1° (EOBBP), and 2.2° (BMOBBP), respectively.

The synthesized ligands **1**, **2**, and **3** were subsequently doubly metallated with six different transition metals (Scheme 3), and products systematically investigated by ion mobility spectrometry and DFT calculations. In total, 18 cofacial homobimetallic complexes could be synthesized and characterized by this new method, out of which 16 compounds were unpublished. Additionally, we were able to grow single crystals of compound **24**, shown in Figure 3, which represents the first unsymmetrical cofacial benzene-linked metalloporphyrin dimer.

Interestingly, X-ray diffraction data of the single crystal show two crystallographically independent but identical molecules in the asymmetric unit. The respective chiral space group is *P*2$_1$ ("Sohncke space group") but crystallized as a twin containing both enantiomers. Compound **24** was refined as an inversion twin with BASF = 0.38(2) (Hooft's *y*-parameter) *y* = 0.39(1).[23] Therefore, the abundance ratio between the two enantiomers in the measured crystal was approximately 62:38. The unit cell of **24** contains two crystallographically independent molecules with identical chirality in an asymmetric unit (see least-squares fit (L.S.-fit) in the Supporting Information, which resembles two "Pac-Man" characters biting each other). The missing phenyl ring opposite to the backbone of one of the two porphyrins enables this curious packing, which disables direct dispersion interactions between the intramolecular

Scheme 2. Synthesis of the monomeric porphyrins covalently linked to the phenyl backbone (**13**–**15**): a) 2-formylphenylboronic acid, Pd(PPh$_3$)$_4$, K$_3$PO$_4$, THF, 80 °C, 6–23 h, **13**: 68%, **14**: 57%, **15**: 52%. Syntheses of cofacial porphyrin dimers (**1**–**3**): b) pyrrole (14.2 equiv), benzaldehyde (9.15 equiv), TFA (1.08 equiv), RT, 115 h, 17%; c) pyrrole (6.07 equiv), benzaldehyde (3.93 equiv), BF$_3$OEt$_2$ (3.47 equiv), RT, 21.5 h, 16%; d) pyrrole (14.1 equiv), benzaldehyde (9.13 equiv), TFA (3.21 equiv), RT, 46 h, 4.7%.
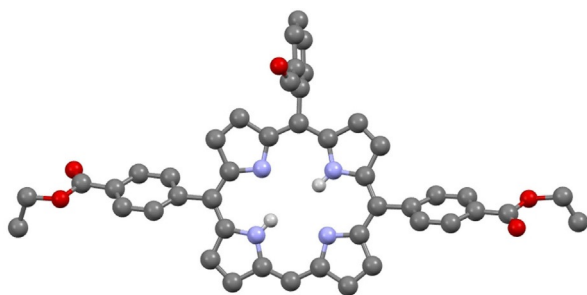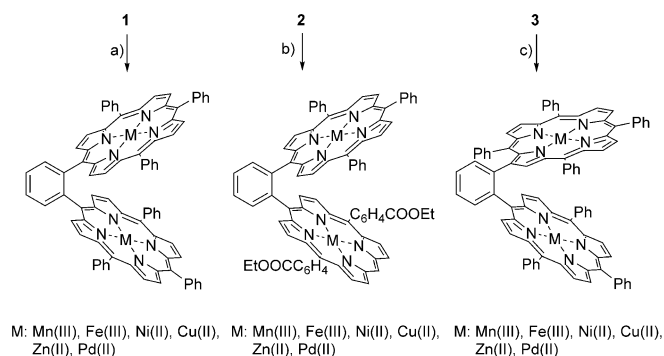
Figure 2. Single-crystal X-ray structure of **14**. For clarity, only the hydrogen atoms bound to nitrogen atoms are displayed.

Chemistry–A European Journal

Full Paper
doi.org/10.1002/chem.202002394

Chemistry Europe
European Chemical
Societies Publishing

Scheme 3. Porphyrin-based homobimetallic complexes: a) (**16**) *Mn^{III}: MnCl$_2$, DMF, 150 °C, 2 h, 86%; (**17**) **Fe^{III}: FeBr$_2$, HCl, DMF, 140 °C, 1 h, 93%; (**18**) Ni^{II}: Ni(acac)$_2$, DMF, 100 °C, 19.5 h, 86%; (**19**) Cu^{II}: Cu(OAc)$_2$, CHCl$_3$/MeOH, 80 °C, 2 h, 93%; (**20**) Zn^{II}: Zn(OAc)$_2$, CHCl$_3$/MeOH, RT, 1 h, 72%; (**21**) Pd^{II}: PdCl$_2$, DMF, 100 °C, 19.5 h, 69%; b) (**22**) *Mn^{III}: MnCl$_2$, DMF, 150 °C, 22 h, 73%; (**23**) **Fe^{III}: FeBr$_2$, HCl, DMF, 140 °C, 2 h, 93%; (**24**) Ni^{II}: Ni(acac)$_2$, DMF, 100 °C, 2 h, 96%; (**25**) Cu^{II}: Cu(OAc)$_2$, CHCl$_3$/MeOH, 80 °C, 1 h, 90%; (**26**) Zn^{II}: Zn(OAc)$_2$, CHCl$_3$/MeOH, 80 °C, 1 h, 99%; (**27**) Pd^{II}: PdCl$_2$, DMF, 80 °C, 20 h, 98%; c) (**28**) *Mn^{III}: MnCl$_2$, DMF, 130 °C, 15.5 h, 79%; (**29**) **Fe^{III}: FeCl$_2$, DMF, 150 °C, 14 h, 87%; (**30**) Ni^{II}: Ni(acac)$_2$, DMF, 150 °C, 5 h, 76%; (**31**) Cu^{II}: Cu(OAc)$_2$, DMF, 60 °C, 4 h, 93%; (**32**) Zn^{II}: Zn(OAc)$_2$, CHCl$_3$/MeOH, RT, 1 h, 95%; (**33**) Pd^{II}: PdCl$_2$, DMF, 100 °C, 3 h, 99%. *Was obtained with two coordinated chlorides at the manganese centers. **Was obtained as the μ-oxido complex.
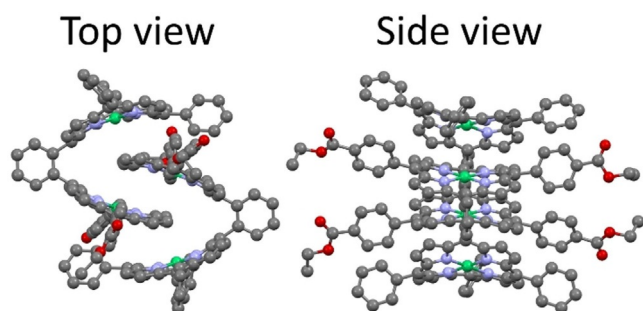

Figure 3. Crystal structure of Ni$^{II}_2$EOBBP **24**. The X-ray diffraction of the single crystal shows two crystallographically independent but identical molecules. The missing phenyl ring opposite to the backbone of one porphyrin subunit per porphyrin dimer enables intermolecular π-stacking. See the Supporting Information (Section 6. Crystallographic Data) for a more detailed description. All hydrogen atoms are omitted for clarity.

porphyrin planes (in contrast to the system reported by Osuka et al.,[17] which has fewer sterically demanding peripheral substituents and can therefore collapse into a cofacial structure with a significantly strained 1,2-biphenylene link in the crystalline solid). An interdigitated arrangement such as in **24** can also overcome the difficulties of growing single crystals of enantiomeric mixtures, which was often problematic in the past. Note that the interdigitated structure in solid state very likely does not correspond to the situation in liquid (or gas) phase, as shown later in the structure determination part. Due to that, we cannot make statements regarding the metal–metal distances in solution. Additionally, the chiral conformers are only distinguishable in solid state because the low interconversion barrier leads to averaging dihedral angles between the porphyrin planes. Nonetheless, all derivatives of **3** are

chiral due to intrinsic planar chirality based on the unsymmetrical linkage to the linker benzene moiety.

Heterobimetallic complexes

As mentioned in the introduction, the demand for tailor-made heterobimetallic complexes as artificial active site analogues of enzymes is huge. Our synthetic approach provides for a new facile route to an artificially synthesized carbon monoxide dehydrogenase active site analogue containing Ni^{II} and Fe^{III}-cations. For this, the following synthetic route was developed as a proof-of-principle reaction to achieve a porphyrin-based transition-metal-containing heterobimetallic complexes. After a Suzuki–Miyaura cross-coupling reaction, the monomeric porphyrin **13** was treated with Ni(acac)$_2$ at 150 °C for 4 h, to obtain the Ni^{II} complex **34** in 72% yield (Scheme 4). Complexation of the Ni^{II} cation can be proven by missing NH protons and slightly increased coupling constants of the β protons adjacent to the 2-formyl-benzene residue from $^3J = 4.8$ to $^3J = 5.0$ Hz, as observed in the corresponding ^{1}H NMR spectra. Through a subsequently performed condensation reaction similar to that shown in Scheme 2, the Ni^{II}-H$_2$-o-phenylene-bisporphyrin **35** can then be obtained in 15% yield. The ring current of the Ni^{II}-containing porphyrin affects the free-base porphyrin in shifting the NH protons to −3.82 ppm, which is typical for cofacially linked porphyrin dimers. The remaining free-base porphyrin in complex **35** can undergo a reaction with FeCl$_2$ in DMF at 150 °C for 4 h to incorporate Fe^{III} as the second cation in 95% yield. The overall yield to obtain the first cofacial porphyrin-based heterobimetallic complex **36** is 2.2% beginning with pyrrole and benzaldehyde as starting material and proves the robustness of the developed synthetic methodology. Based on the results shown, one can expect this protocol to be suitable for many other analogous homo- and heterobimetallic complexes which can find multiple applications in fields ranging from magnetism/spintronics, catalysis, and optical sen-
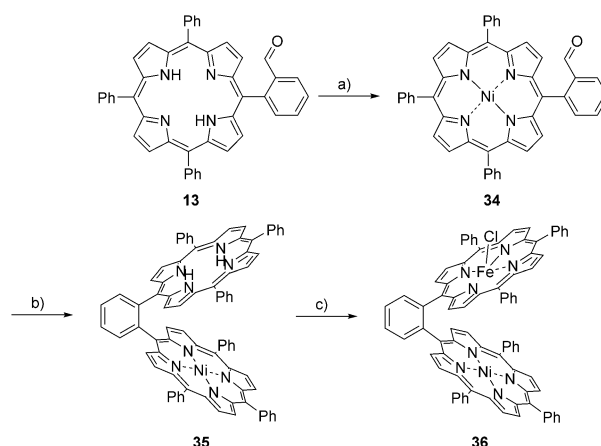
Scheme 4. Synthesis of an artificial carbon monoxide dehydrogenase active site analogue (**36**) through porphyrin building on the monomeric Ni^{II}-containing porphyrin (**34**) and subsequent insertion of Fe^{III} in the second porphyrin ring: a) Ni(acac)$_2$, 150 °C, 4 h, 71%; b) pyrrole, benzaldehyde, TFA, DDQ, RT, 16 h, 15%; c) FeCl$_2$, 150 °C, 4 h, 95%.

sors. Furthermore, the impact of cooperative interactions between (different) spatially proximate metal ions is of fundamental interest, e.g., for enzymatic reactivity in vivo.

Structure determination and UV/Vis spectra

While the above-mentioned complexes have all been well characterized by MS, ^{13}C NMR, ^1H NMR, UV/Vis (Figure 4) and IR spectroscopy, their 3D structure could not be established by the standard structure determination method, X-ray diffraction, due to crystallization problems (except for **24**, see above). Furthermore, we expect that in solid phase, packing effects and intermolecular interactions significantly disrupt the rather delicate balance between π-stacking and van der Waals attraction of porphyrinic moieties on the one hand and Coulomb repulsion of the positively charged metal centers on the other. As a consequence, we applied a combination of quantum chemical calculations and ion mobility spectrometry (IMS) to gain access to at least some structural parameters of corresponding isolated monocations such as the average distance of the porphyrin
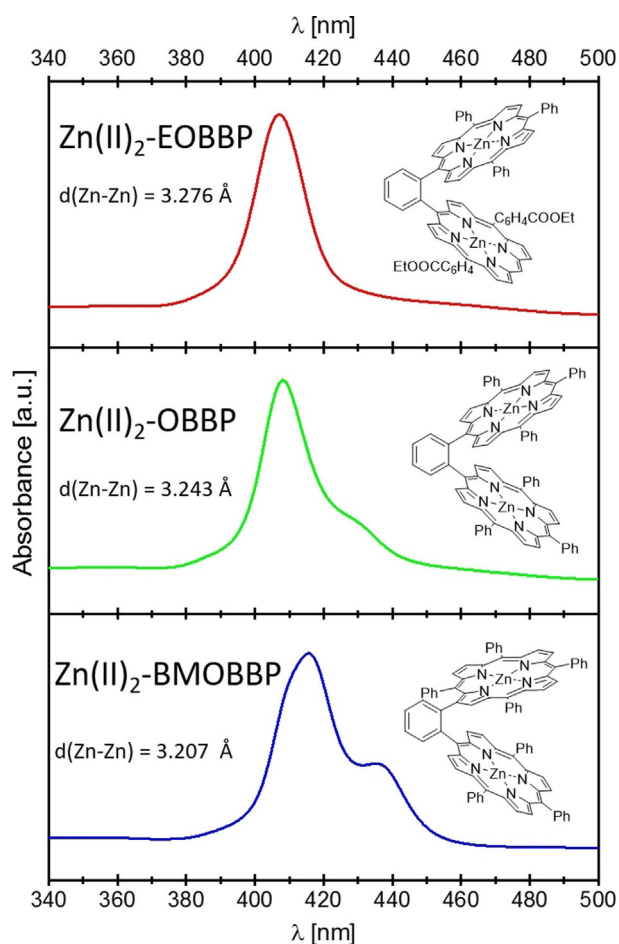
rings. IMS is a gas-phase method to determine the collision cross-section (CCS) of an ion, which can be easily combined with MS.[24] It relies on determination of the drift time of an ion in an inert collision gas (typically helium or nitrogen) guided by an electrical field. With the recent development of several instrumental variants which can provide greatly improved IMS resolution, the method has gained in importance, for example, in studies of proteins,[25] polysaccharides,[26] and fullerenes,[27] and can now provide an additional useful identification parameter in proteomics.[28] In our measurements, we used a high-resolution variant of IMS, trapped ion mobility spectrometry (TIMS) coupled with a ToF-mass spectrometer (timsTOF™, Bruker). The operational mode of TIMS has been described elsewhere.[29] Details regarding the IMS measurements and calculations can be found in the Supporting Information. In brief, with this method, it is possible to differentiate between isomers or conformers that differ in CCS by less than 0.5%. Besides isomer separation, measured CCS can be used to validate structure predictions based on quantum chemical calculations (and collision gas scattering trajectory calculations) and thus to obtain a first-order structural assignment. In detail, the methodology we applied is as follows: For each porphyrin complex we performed a DFT-based geometry optimization (Turbomole package,[30] BP-86 functional,[31,32] def2-SVP basis set,[33] Grimme D3-BJ dispersion correction[34,35]). The partial charges were calculated by the Mulliken algorithm and the CCS calculations were conducted with the IMoS package.[36,37] The coordinates of the Zn^{II}_2 dimers are given in Supporting Information Section 5.2. The optimization was performed for isolated cations, without counterions or solvation effects. Based on these optimized structures we calculated CCS with the trajectory method, which are listed in Table 1. As is evident, all measured CCS values for the covalently linked porphyrin dimers prepared in this study differ by only a few percent from the value of $[(H_2TPP)_2 + H]^+$. Finally, we compared its calculated CCS with the measured CCS. The structures of noncovalently linked TPP dimers are published.[38] We thus determined a scaling factor of 0.94. Note that the calculated CCS depends on both geometry and charge distribution as well as the assumed Lennard–Jones parameters of the constituting atoms. The interplay between these factors is rather delicate, and deviations of several

Figure 4. UV/Vis spectra of the various Zn^{II}_2 dimers. Both OBBP and BMOBBP show a second absorption band in the Soret region that is redshifted by roughly 20 nm relative to the band of highest intensity. Additionally, the most intense band of BMOBBP is redshifted by about 7 nm relative to OBBP. We attribute these shifts (and splittings) to different distances between the Zn^{II} cations.

Table 1. Experimental $^{TIMS}CCS_{N2}$ values of the different porphyrin dimers.

Central atoms	$^{TIMS}CCS_{N2}$ [Å^2][a]			
	OBBP	EOBBP	BMOBBP	TPP dimer
$2H_2 + H$	339.7 ± 0.2	365.9 ± 1.2	350.3 ± 0.4	354.2 ± 0.5
$Mn^{III}_2 + Cl$	345.8 ± 0.8	370.3 ± 0.1	357.8 ± 0.1	
$Fe^{III}_2 + O$	338.1 ± 0.4	362.7 ± 1.3	347.8 ± 0.4	
Ni^{II}_2	337.5 ± 0.4	362.4 ± 0.6	351.0 ± 0.7	
Cu^{II}_2	336.1 ± 0.4	363.8 ± 1.1	350.8 ± 0.1	
Zn^{II}_2	334.9 ± 1.2	360.5 ± 0.7	352.2 ± 0.3	
Pd^{II}_2	335.5 ± 0.1	361.8 ± 1.9	348.7 ± 1.1	
$Ni^{II}H_2 + H$	338.0 ± 0.1			
$Ni^{II}Fe^{III}$		335.5 ± 1.2		

[a] Values are the mean $\pm$ standard deviation of $n = 2$–4 independent measurements.

Chemistry–A European Journal

Full Paper
doi.org/10.1002/chem.202002394

Chemistry
Europe
European Chemical
Societies Publishing

percent between experimental and absolute theoretical CCS are not unusual. A common strategy enabling a better comparison with theory is to calibrate against a well-studied internal standard with a similar structure such as $[(H_2TPP)_2+H]^+$ (Figure 5). After applying this scaling factor to the theoretical CCS of $[Zn^{II}_2\text{-OBBP}]^+$, $[Zn^{II}_2\text{-EOBBP}]^+$ and $[Zn^{II}_2\text{-BMOBBP}]^+$, we reached a deviation between theory and experiment of below 2% (see Table 2 for details). We therefore conclude that our DFT geometries are quite close to the actual structures for all dimers studied, as (OBBP < BMOBBP < EOBBP). The complexes with divalent metal centers (Ni^{II}, Cu^{II}, Zn^{II}, Pd^{II}) show the same CCS, indicating that the nature of the complexed metal does not significantly influence three-dimensional structures. The CCS of the trivalent Mn^{III} dimers, on the other hand, are systematically larger due to the additional Cl^- ion located between the respective metal atoms, which pushes the monomers a bit further apart. The structure of Fe^{III} dimers binding oxygen is analogous, as previously reported.[15]

Based on the DFT-optimized structures of the Zn^{II} dimers (with trends validated by TIMS measurements), we obtain metal-to-metal distances that decrease from EOBBP (3.276 Å) to OBBP (3.243 Å) to BMOBBP (3.207 Å); see Figure 6. Because these correspond to the metal–metal distances of gaseous ions at 0 K, the absolute numbers do not necessarily describe the intramolecular metal center separations in solution or solid, but we assume that even for these condensed phase environments the trend toward decreasing metal center separation in going from EOBBP to BMOBBP will remain the same. Interestingly, the sequence correlates with the increasing prominence of a shoulder (near 435 nm) in the Soret band region of the UV/Vis spectrum. Furthermore, the UV/Vis spectrum of
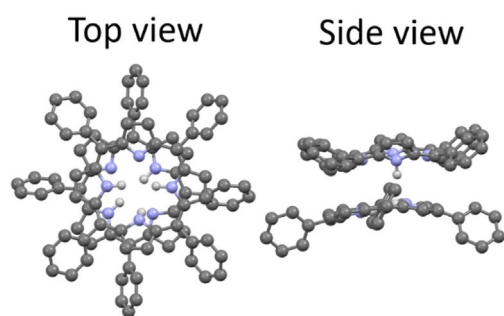

Figure 5. The DFT-calculated structure of $[(H_2TPP)_2+H]^+$ is shown in front and side views. For clarity, only the hydrogen atoms bound to nitrogen atoms are displayed.

Table 2. Experimental CCS and their scaled, theoretical counterparts are listed along with their corresponding deviation.[a]

	Measured CCS [Å²]	Scaled CCS [Å²]	Deviation [%]
$[(H_2TPP)_2+H]^+$	354.2	354.2	calibrant
$[Zn^{II}_2\text{-OBBP}]^+$	334.9	329.7	1.6
$[Zn^{II}_2\text{-EOBBP}]^+$	360.5	362.1	−0.4
$[Zn^{II}_2\text{-BMOBBP}]^+$	352.2	345.6	1.9

[a] As can be seen, the difference between experiment and theory is below 2%, and therefore in good agreement.
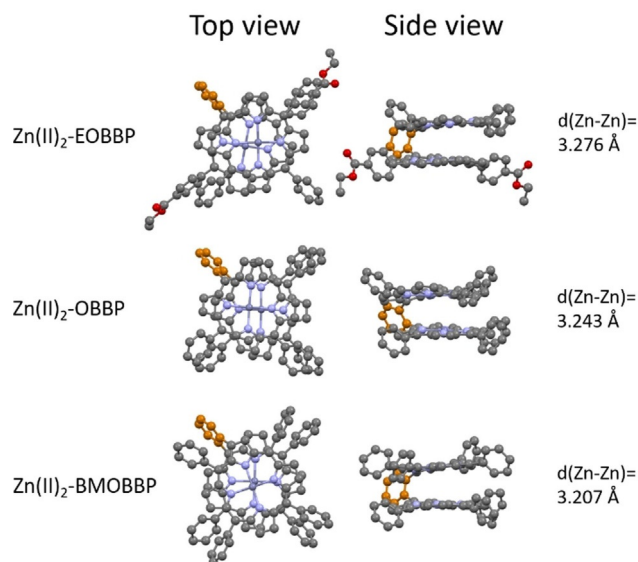

Figure 6. The DFT-calculated structures of the Zn^{II}_2 dimers are shown in front and side views. The values on the right show the calculated distances of the two Zn^{II} cations in each dimer. For clarity, only the hydrogen atoms bound to nitrogen atoms are displayed. The linking phenyl ring is drawn in orange for clarity as well. The coordinates are included in x,y,z format in Section 5.2 of the Supporting Information.

$[Zn^{II}_2\text{-BMOBBP}]$ shows a broadening and slight asymmetry of the Soret band, which might indicate an additional absorption band. We tentatively assign this to enhanced spatial π-interaction and hence stronger coupling between the chromophores as the intermetal distance decreases. In a 2018 study, Jäger et al. investigated the changes in the Q-band absorption region of gaseous dimeric porphyrin ions, which were induced by structural differences.[39] In the case of isolated Zn^{II}_2 dimers, analogous shifts of Q-band peak maxima by up to 8 nm were reported.

This is consistent with a previous related study by Takai et al. who showed, that increasing distances between the two monomers of a porphyrin dimer also increases the reorganization energies associated with electron transfer between the chromophores, proving that the distance can change the properties of porphyrin dimers and presumably higher oligomers as well.[40] Furthermore, Bolze et al. showed that covalently linked dimers of Pd^{II} porphyrins and monomers of Pd^{II} porphyrins can differ in their Q-band region absorption quite drastically (the Soret region was not shown).[41]

The slight decrease of metal center distance between Zn^{II}_2-EOBBP and Zn^{II}_2-OBBP can be attributed to enhanced attractive interaction between proximal phenyl rings of the porphyrin dimers (whereas EOBBP lacks some corresponding phenyls). Compared with Zn^{II}_2-OBBP, the phenyls of the two porphyrin rings of Zn^{II}_2-BMOBBP can be better intercalated. Thus the separation of the metals can be decreased further.

Conclusions

We present a straightforward new synthesis route for both homo- and heterobimetallic porphyrin complexes. The proto-

Chemistry–A European Journal

Full Paper
doi.org/10.1002/chem.202002394

Chemistry Europe
European Chemical
Societies Publishing

col allows the synthesis of aryl-based *meso-meso* as well as β-*meso*-linked porphyrins with an optional phenyl residue on one of the porphyrin subunits. Where comparisons with literature can be drawn, the developed methodology generally provides higher yields, for example, by a factor of 6.8 for the well-known symmetric porphyrin dimer **1**. Based on this improved accessibility we synthesized 18 different homobimetallic species containing the transition metals Mn^{III}, Fe^{III}, Ni^{II}, Cu^{II}, Zn^{II}, and Pd^{II}. In the case of Ni^{II} and Fe^{III} we were able to prepare heterobimetallic species. The isolated species were characterized by ^1H NMR, ^{13}C NMR, UV/Vis, IR, MS, and high-resolution IMS measurements, which were contrasted with DFT calculations. For a set of three different bimetallic Zn^{II} complexes, we could show that metal–metal distances differ systematically with ligand (due to steric effects) and were able to correlate this trend with Soret band shifts and splitting. Furthermore, an unsymmetrical Ni^{II}_2 complex could be crystallized in the form of a twin containing both planar-chiral enantiomers. Thus we were able to obtain the first single-crystal X-ray structure of an unsymmetrical cofacial benzene-linked porphyrin dimer.

Experimental Section

The synthetic procedures for all synthesized compounds are available in the Supporting Information. Deposition Number 1988039 (compound **24**) contains the supplementary crystallographic data for this paper. These data are provided free of charge by the joint Cambridge Crystallographic Data Centre and Fachinformationszentrum Karlsruhe Access Structures service: www.ccdc.cam.ac.uk/structures. Due to the poor quality of the data for **14**, these were not deposited with The Cambridge Crystallographic Data Centre.

Acknowledgements

Conflict of interest

The authors declare no conflict of interest.

[1] J. Brown, L. Powers, B. Kincaid, J. Larrabee, T. G. Spiro, *J. Am. Chem. Soc.* **1980**, *102*, 4210–4216.
[2] K. Tatsumi, R. Hoffmann, *J. Am. Chem. Soc.* **1981**, *103*, 3328–3341.
[3] I. M. Klotz, T. A. Klotz, H. A. Fiess, *Arch. Biochem. Biophys.* **1957**, *68*, 284–299.
[4] A. Desideri, M. Falconi, F. Polticelli, M. Bolognesi, K. Djinovic, G. Rotilio, *J. Mol. Biol.* **1992**, *223*, 337–342.
[5] H. Dobbek, V. Svetlitchnyi, L. Gremer, R. Huber, O. Meyer, *Science* **2001**, *293*, 1281–1285.
[6] J. P. Collman, N. K. Devaraj, R. A. Decréau, Y. Yang, Y.-L. Yan, W. Ebina, T. A. Eberspacher, C. E. Chidsey, *Science* **2007**, *315*, 1565–1568.
[7] A. Treibs, *Liebig Ann. Chem.* **1969**, *728*, 115–143.
[8] M. O. Senge, *Chem. Commun.* **2011**, *47*, 1943–1960.
[9] C. Chang, *J. Heterocycl. Chem.* **1977**, *14*, 1285–1288.
[10] J. P. Collman, P. Denisevich, Y. Konai, M. Marrocco, C. Koval, F. C. Anson, *J. Am. Chem. Soc.* **1980**, *102*, 6027–6036.
[11] J. T. Landrum, D. Grimmett, K. J. Haller, W. R. Scheidt, C. A. Reed, *J. Am. Chem. Soc.* **1981**, *103*, 2640–2650.
[12] J. P. Collman, C. S. Bencosme, C. E. Barnes, B. D. Miller, *J. Am. Chem. Soc.* **1983**, *105*, 2704–2710.
[13] C. Chang, I. Abdalmuhdi, *J. Org. Chem.* **1983**, *48*, 5388–5390.
[14] C. K. Chang, I. Abdalmuhdi, *Angew. Chem. Int. Ed.* **1984**, *23*, 164–165.
[15] Y. Deng, C. J. Chang, D. G. Nocera, *J. Am. Chem. Soc.* **2000**, *122*, 410–411.
[16] H. Meier, Y. Kobuke, S.-i. Kugimiya, *Chem. Commun.* **1989**, 923–924.
[17] A. Osuka, S. Nakajima, T. Nagata, K. Maruyama, K. Toriumi, *Angew. Chem. Int. Ed.* **1991**, *30*, 582–584.
[18] J. T. Fletcher, M. J. Therien, *J. Am. Chem. Soc.* **2000**, *122*, 12393–12394.
[19] J. T. Fletcher, M. J. Therien, *J. Am. Chem. Soc.* **2002**, *124*, 4298–4311.
[20] L. L. Chng, C. J. Chang, D. G. Nocera, *J. Org. Chem.* **2003**, *68*, 4075–4078.
[21] Y. Shimazaki, H. Takesue, T. Chishiro, F. Tani, Y. Naruta, *Chem. Lett.* **2001**, *30*, 538–539.
[22] H. S. Cho, D. H. Jeong, M.-C. Yoon, Y. H. Kim, Y.-R. Kim, D. Kim, S. C. Jeoung, S. K. Kim, N. Aratani, H. Shinmori, *J. Phys. Chem. A* **2001**, *105*, 4200–4210.
[23] R. W. Hooft, L. H. Straver, A. L. Spek, *J. Appl. Crystallogr.* **2008**, *41*, 96–103.
[24] E. A. Mason, E. W. McDaniel, *NASA STI/Recon Tech. Rep. A* **1988**, *89*, 576.
[25] M. E. Ridgeway, J. A. Silveira, J. E. Meier, M. A. Park, *Analyst* **2015**, *140*, 6964–6972.
[26] Y. Pu, M. E. Ridgeway, R. S. Glaskin, M. A. Park, C. E. Costello, C. Lin, *Anal. Chem.* **2016**, *88*, 3440–3443.
[27] P. Weis, F. Hennrich, R. Fischer, E. K. Schneider, M. Neumaier, M. M. Kappes, *PCCP* **2019**, *21*, 18877–18892.
[28] D. Helm, J. P. Vissers, C. J. Hughes, H. Hahne, B. Ruprecht, F. Pachl, A. Grzyb, K. Richardson, J. Wildgoose, S. K. Maier, *Mol. Cell. Proteomics* **2014**, *13*, 3709–3715.
[29] K. Michelmann, J. A. Silveira, M. E. Ridgeway, M. A. Park, *J. Am. Chem. Mass. Spec.* **2015**, *26*, 14–24.
[30] F. Furche, R. Ahlrichs, C. Hättig, W. Klopper, M. Sierka, F. T. Weigend, *Mol. Sci.* **2014**, *4*, 91–100.
[31] J. P. Perdew, *Phys. Rev. B* **1986**, *33*, 8822.
[32] A. D. Becke, *Phys. Rev. A* **1988**, *38*, 3098.
[33] F. Weigend, R. Ahlrichs, *PCCP* **2005**, *7*, 3297–3305.
[34] S. Grimme, J. Antony, S. Ehrlich, H. Krieg, *J. Chem. Phys.* **2010**, *132*, 154104.
[35] S. Grimme, S. Ehrlich, L. Goerigk, *J. Comput. Chem.* **2011**, *32*, 1456–1465.
[36] C. Larriba, C. J. Hogan, *J. Comput. Phys.* **2013**, *251*, 344–363.
[37] C. Larriba, C. J. Hogan, *J. Phys. Chem. A* **2013**, *117*, 3887–3901.
[38] K. Brendle, U. Schwarz, P. Jäger, P. Weis, M. Kappes, *J. Phys. Chem. A* **2016**, *120*, 8716–8724.

[39] P. Jäger, K. Brendle, E. Schneider, S. Kohaut, M. K. Armbruster, K. Fink, P. Weis, M. M. Kappes, *J. Phys. Chem. A* **2018**, *122*, 2974–2982.

[40] A. Takai, C. P. Gros, J. M. Barbe, R. Guilard, S. Fukuzumi, *Chem. Eur. J.* **2009**, *15*, 3110–3122.

[41] F. Bolze, C. P. Gros, P. D. Harvey, R. Guilard, *J. Porphyrins Phthalocyanines* **2001**, *5*, 569–574.